

# Thermodynamic cost-controllability tradeoff in metabolic currency coupling

Jumpei F. Yamagishi\*

Center for Biosystems Dynamics Research, RIKEN,

6-7-1 Minatojima-minamimachi, Chuo-ku, Kobe 650-0047, Japan and

Universal Biology Institute, The University of Tokyo, 7-3-1 Hongo, Tokyo 113-0033, Japan

Tetsuhiro S. Hatakeyama

Earth-Life Science Institute, Institute of Future Science,

Institute of Science Tokyo, Tokyo 152-8550, Japan

Cellular metabolism is globally regulated by various currency metabolites such as ATP, GTP, and NAD(P)H. These metabolites cycle between charged (high-energy) and uncharged (low-energy) states to mediate energy transfer. While distinct currency metabolites are associated with different metabolic functions, their charged and uncharged forms are generally interchangeable via biochemical reactions such as  $ATP + GDP \rightleftharpoons ADP + GTP$  and  $NADP^+ + NADH \rightleftharpoons NADPH + NAD^+$ . Thus, their energetic states are generally coupled and influence each other, which would hinder the independent regulation of different currency metabolites. Despite the extensive knowledge of the molecular biology of individual currency metabolites, it remains poorly understood how the coordination of various coupled currency metabolites shapes metabolic regulation, efficiency, and ultimately the evolution of organisms. Here, we present a minimal theoretical model of metabolic currency coupling and reveal a fundamental tradeoff relationship between metabolic controllability and thermodynamic cost: increasing the capacity to independently regulate multiple currency metabolites generally requires comparable abundances of those metabolites, which in turn incurs a higher entropy production rate. The tradeoff suggests that in complex environments, organisms evolutionarily favor an equal abundance of currency metabolites to enhance metabolic controllability at the expense of a higher thermodynamic cost; conversely, in simple environments, organisms evolve to have imbalanced amounts of them to reduce heat dissipation. These considerations also offer a hypothesis regarding evolutionary trends in nucleotide-pool balance and genomic GC content.

## I. INTRODUCTION

Living organisms must continually consume energy to maintain their order and avoid reaching thermodynamic equilibrium. In the 1940s, Erwin Schrödinger famously argued that life persists by avoiding equilibrium through metabolism [1, 2]. Since then, cellular metabolism has remained a central topic in the study of nonequilibrium thermodynamics, attracting the interest of physicists and biologists alike [3, 4]. Remarkably, recent advancements in stochastic thermodynamics have provided a rigorous nonequilibrium thermodynamic description for open chemical reaction networks, applicable to general metabolic reaction networks [5–10]. However, most theoretical efforts to date have taken one of two extremes: they either derive very general thermodynamic constraints applicable to arbitrary chemical reaction networks [6, 8, 9], or they analyze specific, simple biochemical processes such as single-enzyme kinetics [11, 12] and molecular machines [13]. A substantial conceptual gap remains between broad theoretical frameworks and detailed, context-specific biochemical studies. To reveal the key biophysical principles of metabolism, we must bridge this gap by developing a coarse-grained theory that preserves the unique characteristics of metabolic systems.

One approach to appropriately coarse-graining the complexity of metabolism is to focus on a special class of compounds that globally mediate energy transfer across many metabolic reactions: *coenzymes*. A coenzyme is a small, non-protein organic compound that associates loosely with enzymes and participates in enzymatic reactions as a transferable carrier of chemical groups or electrons [14, 15]. Well-known examples of coenzymes include adenosine triphosphate (ATP), which carries high-energy phosphate groups, and nicotinamide adenine dinucleotide (NADH/NAD<sup>+</sup>), which carries high-energy electrons. Coenzymes typically cycle between high-energy (charged) and low-energy (uncharged) forms [16–18]. ATP, for instance, is converted by hydrolysis into its lower-energy forms ADP or AMP (adenosine diphosphate or monophosphate), releasing energy, whereas ADP can be recharged back into ATP through processes such as cellular respiration or photosynthesis.

Because of their central role in energy transfer, coenzymes are often referred to as *currency metabolites* or *metabolic currencies* [19, 20]. Much like money in an economy, currency metabolites fulfill Jevons's functions of money [21, 22]: they serve as a medium of exchange (transferring energy or chemical groups), a unit of account (providing a characteristic energy metric across reactions), and a store of value (storing energy). The charged/uncharged ratios of currency metabolites, such as the ATP/ADP ratio, regulate metabolic activity globally and serve as macroscopic indicators of the cellu-

\* jumpei.yamagishi@riken.jp

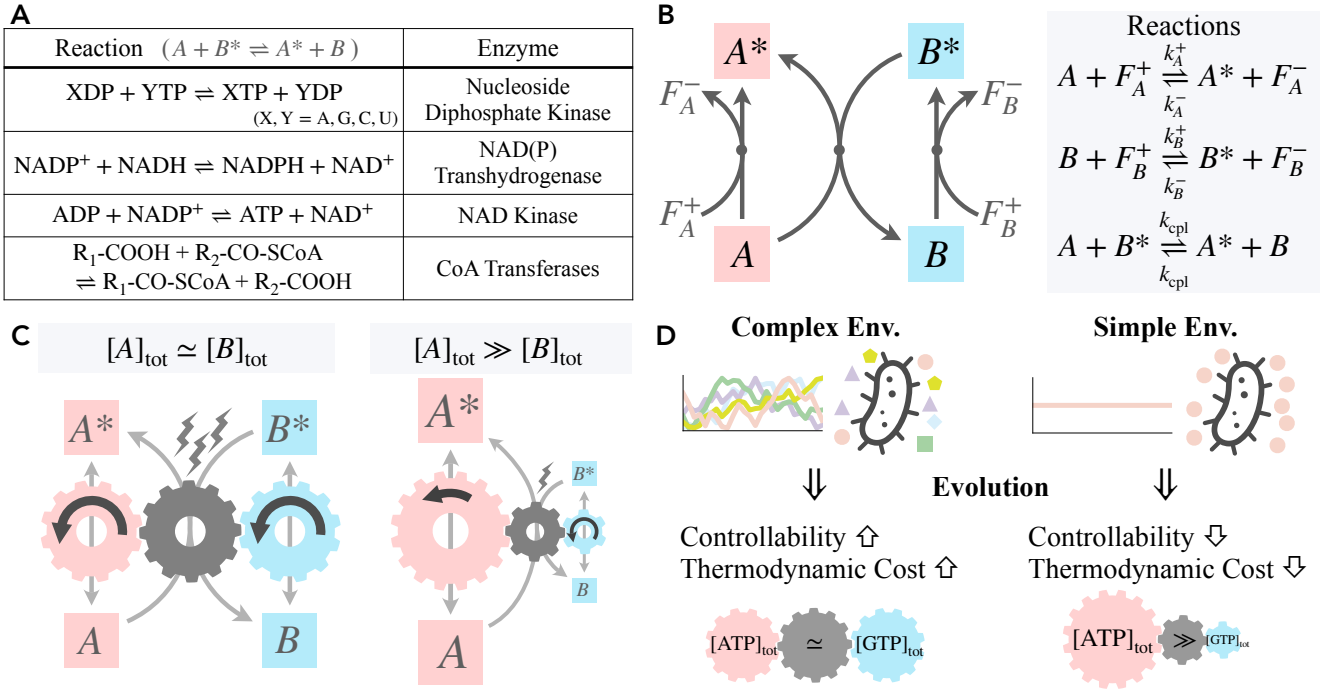


FIG. 1. Metabolic currency coupling. (A) Examples of transferases and their associated currency coupling reactions. (B) Model of the coupling of currency metabolites. All reactions are reversible. Table I collects all the notation in one place. (C) Schematics of how the balance in currency metabolite pools affects metabolic controllability and thermodynamic cost. Coupling reactions cause the ratios  $[A^*]/[A]$  and  $[B^*]/[B]$  to shift in the same direction. The former strongly influences the latter when  $[A]_{\text{tot}} \gg [B]_{\text{tot}}$ . Conversely, a large  $[A]_{\text{tot}}/[B]_{\text{tot}}$  ratio reduces the entropy production rate required to maintain the metabolic currency coupling, which is analogous to the “friction” between different currency metabolites. (D) A theoretical connection between organismal or habitat complexity and pool sizes of multiple currency metabolites.

lar metabolic state [15, 23–25]: a higher ratio biases metabolism toward overall ATP-driven reactions over ADP-driven ones, while a lower ratio favors ADP-driven reactions.

Cellular metabolic systems employ multiple different currency metabolites (e.g., ATP, GTP, NAD(P)H, and acetyl-CoA), each generally associated with specific biochemical functions [25, 26]: for example, ATP is known as the primary energy currency for most biochemical reactions, while GTP works for signaling and protein synthesis processes, such as powering G-proteins and the translation of mRNA [27, 28]; among the electron carriers, NADPH predominantly drives anabolic (biosynthetic) reactions, while NADH feeds into catabolic reactions, such as cellular respiration [29, 30]. Cells are considered to coordinate various metabolic demands separately by allocating different currency metabolites to different tasks.

Despite their distinct roles, the energetic states of different currency metabolites are thermodynamically and chemically coupled rather than isolated. In general, the charged and uncharged forms of distinct currency metabolites can be interconverted through specific enzymatic reactions [16]. For example, nucleoside diphosphate kinase catalyzes a reversible phosphate exchange between nucleoside diphosphates and triphosphates (NDPs and NTPs), effectively linking the

ATP/ADP and GTP/GDP ratios through the reaction  $\text{ATP} + \text{GDP} \rightleftharpoons \text{ADP} + \text{GTP}$  [31]; other transferases (EC 2) perform analogous exchanges (Fig. 1A). Such coupling reactions will hinder the independent regulation of different currency metabolites: if the intracellular ATP/ADP ratio is increased, for instance, coupling reactions will inevitably push the GTP/GDP ratio upward as well.

While extensive knowledge of the molecular biology of individual currency metabolites has been accumulated, how the coordination of various coupled currency metabolites influences metabolic regulation, efficiency, and ultimately the physiology and evolution of organisms remains poorly understood. To address this gap, we theoretically elucidate inherent, system-wide constraints on how cellular metabolism is regulated via metabolic currency coupling.

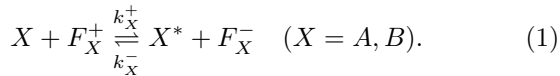
In this study, we develop a minimal theoretical model of metabolic currency coupling. We thereby derive a fundamental tradeoff between metabolic controllability and thermodynamic cost: balanced currency metabolite pools enhance metabolic control at the expense of increased entropy production rate as a thermodynamic cost (see also Fig. 1C). From a biological standpoint, this tradeoff suggests that organisms in complex environments would evolutionarily favor uniformity in currency metabolite pools to increase their metabolic con-

trollability; in contrast, those in simpler environments would evolutionarily favor a skewed distribution of currency pools to reduce the thermodynamic cost (Fig. 1D). We then explore biological and evolutionary implications of this tradeoff, including a hypothetical link between ATP–GTP coupling, organismal complexity, and genomic GC content.

## II. MODEL

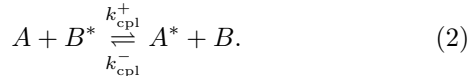
As the simplest case, we consider the coupling of two currency metabolites  $X = A, B$  (see also Fig. 1B and Table I).

Each currency metabolite is driven from its uncharged state  $X$  into its charged state  $X^*$  via a single effective reaction,



Here,  $F_X^+$  coarse-grains a pool of energy-rich “fuel” substrates (e.g., nutrients or reducing equivalents), and  $F_X^-$  represents a lumped set of lower-energy products or waste. Thus, this reversible reaction represents both catabolic (rightward) and anabolic (leftward) processes.

Different currency metabolites interconvert between their charged and uncharged states as



For the sake of simplicity, it is assumed that the difference in standard chemical potentials between  $X^*$  and  $X$ ,  $\Delta\mu_X^o := \mu_{X^*}^o - \mu_X^o > 0$ , is identical for both currency metabolites  $X = A, B$ . From the local detailed balance condition,  $k_{\text{cpl}}^+ = k_{\text{cpl}}^-$  then holds, which will be denoted by  $k_{\text{cpl}}$  hereafter.

Assuming mass action kinetics, the rate equation for this system is given as

$$\begin{aligned} \frac{d}{dt} \begin{pmatrix} [A] \\ [A^*] \\ [B] \\ [B^*] \end{pmatrix} &= \begin{pmatrix} -1 & 0 & -1 \\ 1 & 0 & 1 \\ 0 & -1 & 1 \\ 0 & 1 & -1 \end{pmatrix} \begin{pmatrix} J_A \\ J_B \\ J_{\text{cpl}} \end{pmatrix}, \quad (3) \\ J_A &= \kappa_A^+ [A] - \kappa_A^- [A^*], \\ J_B &= \kappa_B^+ [B] - \kappa_B^- [B^*], \\ J_{\text{cpl}} &= k_{\text{cpl}} [A][B^*] - k_{\text{cpl}} [A^*][B], \end{aligned}$$

where the effective rate constants for the driving reactions, defined as  $\kappa_X^\pm := k_X^\pm [F_X^\pm]$ , quantify how strongly currency metabolite  $X$  is driven into its charged and uncharged state by catabolic and anabolic processes.

Each reaction conserves the total pool of each currency metabolite  $X$ , i.e.,

$$[X]_{\text{tot}} := [X^*] + [X] \quad (X = A, B)$$

TABLE I. Notations

Symbol	Description
$X, X^*$	Currency metabolite in uncharged/charged state ( $X = A, B$ )
$[X]_{\text{tot}}$	Pool size of currency metabolite $X$
$k_{\text{cpl}}$	Rate constant for the coupling reaction (Eq. (2))
$k_X^\pm$	Rate constant for the driving reactions (Eq. (1))
$F_X^\pm$	Fuel ( $F_X^+$ ) and product ( $F_X^-$ ) for the driving reactions
$\kappa_X^\pm, \kappa_X$	Effective rate constant for the driving reactions ( $\kappa_X^\pm := k_X^\pm [F_X^\pm]$ ; $\kappa_X := \kappa_X^+ + \kappa_X^-$ )
$\Gamma_X$	Charged/Uncharged ratio of $X$ ( $\Gamma_X := [X^*]/[X]$ )
$\Gamma_0$	$\Gamma_X$ in the strong coupling limit (Eq. (5))
$e_{XY}^\pm$	Elasticity of $\Gamma_X$ by $\kappa_Y^\pm$ (Eq. (6))
$e_X$	Geometric mean of $e_{XX}^\pm$ (Eq. (13))
$e$	Mean elasticity (Eq. (14))
$\tilde{e}_X^\pm$	$\tilde{e}_X^\pm$ in strong coupling limit
$\sigma_{\text{cpl}}$	Entropy production rate (EPR) of the coupling reaction

are conserved moieties. By exploiting the symmetry between currency metabolites, we order their total pool sizes as  $[A]_{\text{tot}} \geq [B]_{\text{tot}}$ , unless otherwise stated.

## III. RESULTS

The present study focuses on the charged/uncharged ratios of currency metabolites  $X$ ,  $\Gamma_X := [X^*]/[X]$ . These ratios determine the macroscopic state of intracellular metabolism: when  $\Gamma_X$  increases (decreases), the net fluxes of  $X^*$ -driven reactions are preferentially promoted (suppressed) overall.

First,  $\Gamma_X$  at the steady state, denoted by  $\Gamma_X^{\text{st}}$ , is calculated as (see also Appendix A):

$$\begin{aligned} \Gamma_A^{\text{st}} &= \frac{[A^*]^{\text{st}}}{[A]^{\text{st}}} = \frac{k_{\text{cpl}} [A]_{\text{tot}} \kappa_A^+ + k_{\text{cpl}} [B]_{\text{tot}} \kappa_B^+ + \kappa_A^+ \kappa_B^-}{k_{\text{cpl}} [A]_{\text{tot}} \kappa_A^- + k_{\text{cpl}} [B]_{\text{tot}} \kappa_B^- + \kappa_A^- \kappa_B^+}, \\ \Gamma_B^{\text{st}} &= \frac{[B^*]^{\text{st}}}{[B]^{\text{st}}} = \frac{k_{\text{cpl}} [A]_{\text{tot}} \kappa_A^+ + k_{\text{cpl}} [B]_{\text{tot}} \kappa_B^+ + \kappa_A^- \kappa_B^+}{k_{\text{cpl}} [A]_{\text{tot}} \kappa_A^- + k_{\text{cpl}} [B]_{\text{tot}} \kappa_B^- + \kappa_A^+ \kappa_B^-}, \end{aligned} \quad (4)$$

where  $\kappa_X := \kappa_X^+ + \kappa_X^-$  (see also Fig. 2A). Without currency coupling (i.e.,  $k_{\text{cpl}} = 0$ )  $\Gamma_X^{\text{st}} = \kappa_X^+ / \kappa_X^-$  holds, as the coupling reaction deviates  $\Gamma_X^{\text{st}}$  from the  $\kappa_X^+ / \kappa_X^-$  ratio. This deviation depends on the pool size  $[Y]_{\text{tot}}$  of the other currency metabolite  $Y (\neq X)$  as well as the coupling constant  $k_{\text{cpl}}$ . In the limit of weak currency coupling,  $k_{\text{cpl}} \ll \kappa_X^\pm / [X]_{\text{tot}}$ ,

$$\Gamma_X^{\text{st}} = \frac{\kappa_X^+}{\kappa_X^-} + k_{\text{cpl}} [Y]_{\text{tot}} \frac{\kappa_Y^-}{\kappa_Y \kappa_X^-} \left( \frac{\kappa_Y^+}{\kappa_Y^-} - \frac{\kappa_X^+}{\kappa_X^-} \right) + O(k_{\text{cpl}}^2).$$

As  $[Y]_{\text{tot}}$  increases,  $\Gamma_X^{\text{st}}$  deviates more from  $\kappa_X^+ / \kappa_X^-$  toward  $\kappa_Y^+ / \kappa_Y^-$ .

By contrast, in the strong coupling limit,  $k_{\text{cpl}} \gg \kappa_X^\pm / [X]_{\text{tot}}$ , both steady-state ratios  $\Gamma_A^{\text{st}}$  and  $\Gamma_B^{\text{st}}$  collapse onto a single value as

$$\Gamma_X^{\text{st}} \rightarrow \Gamma_0 := \frac{[A]_{\text{tot}} \kappa_A^+ + [B]_{\text{tot}} \kappa_B^+}{[A]_{\text{tot}} \kappa_A^- + [B]_{\text{tot}} \kappa_B^-} \quad (X = A, B), \quad (5)$$

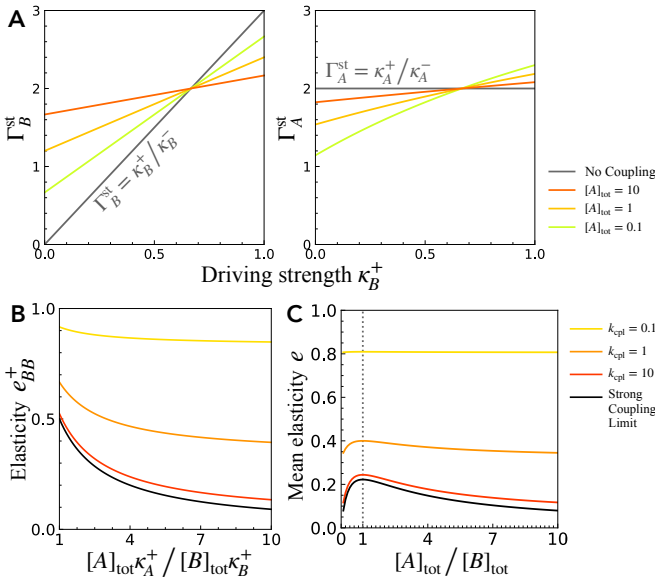


FIG. 2. Elasticity of the charged/uncharged ratios with metabolic currency coupling. (A) Dependence of charged/uncharged ratio  $\Gamma_X^{\text{st}}$  ( $X = A, B$ ) on  $\kappa_B^+$ . Colored lines show the cases with  $k_{\text{cpl}} = 1$ ,  $[B]_{\text{tot}} = 1$  and different  $[A]_{\text{tot}}$ , while gray line shows the no coupling case. (B) Dependence of self-elasticity  $e_B^+$  on  $[A]_{\text{tot}} \kappa_A^+ / [B]_{\text{tot}} \kappa_B^+$ . Colored lines show different coupling strength  $k_{\text{cpl}}$  and black line shows the large coupling limit,  $\tilde{e}_B^+$  (Eq. (11)). (C) Relationship between  $[A]_{\text{tot}} / [B]_{\text{tot}}$  and mean elasticity  $e$ . The black line shows the strong coupling limit. In panels (B) and (C),  $\kappa_B^+ = 1/3$  and  $[A]_{\text{tot}} + [B]_{\text{tot}} = 2$  are fixed. The other parameters are set as  $\kappa_A^+ = 2/3$ ,  $\kappa_A^- = 1/3$ , and  $\kappa_B^- = 2/3$ .

which is a weighted average of the individual driving force ratios  $\kappa_X^+ / \kappa_X^-$  with weights  $[X]_{\text{tot}}$ . With strong currency coupling, the relative size of the currency pools determines the charged/uncharged ratio,  $\Gamma_X^{\text{st}}$ .

### A. Controllability of charged/uncharged ratios

The adaptive regulation of cellular metabolism requires the appropriate modulation of the charged/uncharged ratios  $\Gamma_X$  in response to changing environmental conditions such as nutrient availability. To quantify this controllability, we adopt the concept of *elasticity* from economics [32], measuring the susceptibility of the steady-state charged/uncharged ratios  $\Gamma_X^{\text{st}}$  to variations in the effective rate constant for a driving reaction,  $\kappa_Y^{\pm}$ :

$$e_{XY}^{\pm} := \pm \frac{\partial \log \Gamma_X^{\text{st}}}{\partial \log \kappa_Y^{\pm}} \quad (X, Y = A, B). \quad (6)$$

where it is defined in logarithmic form to be dimensionless. As  $\Gamma_X^{\text{st}}$  ( $1/\Gamma_X^{\text{st}}$ ) increases linearly with the driving strength  $\kappa_X^+$  ( $\kappa_X^-$ ) as shown in Eq. (4), each elasticity  $e_{XY}^{\pm}$

takes a constant, dimensionless value between 0 and 1:

$$e_{AA}^{\pm} = \frac{k_{\text{cpl}}[A]_{\text{tot}} \kappa_A^{\pm} + \kappa_A^{\pm} \kappa_B}{k_{\text{cpl}}[A]_{\text{tot}} \kappa_A^{\pm} + k_{\text{cpl}}[B]_{\text{tot}} \kappa_B^{\pm} + \kappa_A^{\pm} \kappa_B}, \quad (7)$$

$$e_{AB}^{\pm} = \frac{k_{\text{cpl}}[B]_{\text{tot}} \kappa_B^{\pm}}{k_{\text{cpl}}[A]_{\text{tot}} \kappa_A^{\pm} + k_{\text{cpl}}[B]_{\text{tot}} \kappa_B^{\pm} + \kappa_A^{\pm} \kappa_B}, \quad (8)$$

$$e_{BA}^{\pm} = \frac{k_{\text{cpl}}[A]_{\text{tot}} \kappa_A^{\pm}}{k_{\text{cpl}}[A]_{\text{tot}} \kappa_A^{\pm} + k_{\text{cpl}}[B]_{\text{tot}} \kappa_B^{\pm} + \kappa_A \kappa_B^{\pm}}, \quad (9)$$

$$e_{BB}^{\pm} = \frac{k_{\text{cpl}}[B]_{\text{tot}} \kappa_B^{\pm} + \kappa_A \kappa_B^{\pm}}{k_{\text{cpl}}[A]_{\text{tot}} \kappa_A^{\pm} + k_{\text{cpl}}[B]_{\text{tot}} \kappa_B^{\pm} + \kappa_A \kappa_B^{\pm}}. \quad (10)$$

Note that the elasticity of  $\Gamma_X^{\text{st}}$  against different driving reactions satisfies  $e_{XA}^{\pm} + e_{XB}^{\pm} = 1$  ( $X = A, B$ ).

Equations (7)-(10) show that elasticity is governed not only by the rate constants for the driving and coupling reactions,  $\kappa_X^{\pm}$  and  $k_{\text{cpl}}$ , but also by the currency metabolite pool sizes,  $[X]_{\text{tot}}$  (Fig. 2B). In particular, each elasticity  $e_{XY}^{\pm}$  depends on the relative magnitude of  $[X]_{\text{tot}} \kappa_X^{\pm}$ . This is particularly evident in the strong coupling limit,  $k_{\text{cpl}} \gg \kappa_X^{\pm} / [X]_{\text{tot}}$ :

$$e_{YX}^{\pm} \rightarrow \tilde{e}_X^{\pm} := \frac{[X]_{\text{tot}} \kappa_X^{\pm}}{[A]_{\text{tot}} \kappa_A^{\pm} + [B]_{\text{tot}} \kappa_B^{\pm}}. \quad (11)$$

This  $\tilde{e}_X^{\pm}$  satisfies

$$e_{XX}^{\pm} \geq \tilde{e}_X^{\pm} \geq e_{YX}^{\pm} \quad (Y \neq X), \quad (12)$$

and it thus provides the lower (upper) bound of the dimensionless elasticity  $e_{XX}^{\pm}$  ( $e_{YX}^{\pm}$ ) (see also Fig. 2B).

Remarkably, when the currency metabolite pools become imbalanced ( $[A]_{\text{tot}} \gg [B]_{\text{tot}}$ ), the less abundant currency  $B$  loses susceptibility to its own drives  $\kappa_B^{\pm}$  and becomes predominantly slaved to  $\Gamma_A^{\text{st}}$  and  $\kappa_A^{\pm}$  (Fig. 2AB). In other words, the model effectively behaves as a single-degree-of-freedom system. Intuitively, this occurs because the more abundant currency metabolite  $A$  acts as a chemical bath against the less abundant currency metabolite  $B$  (Fig. 1C).

Taking the geometric mean of “self-elasticity”  $e_{XX}^{\pm}$  yields a single measure of the controllability of each  $\Gamma_X^{\text{st}}$ :

$$e_X := \sqrt{e_{XX}^+ e_{XX}^-} \quad (X = A, B). \quad (13)$$

Furthermore, the geometric mean of  $e_X$  yields a single measure of the system-wide controllability:

$$e := \sqrt{e_A e_B} = (e_{AA}^+ e_{AA}^- e_{BB}^+ e_{BB}^-)^{1/4}. \quad (14)$$

Consistent with the above discussion, imbalanced currency metabolite pools ( $[A]_{\text{tot}} \gg [B]_{\text{tot}}$ ) bias  $e_{XX}^{\pm}$ , and consequently  $e_X$ , thereby reducing mean elasticity  $e$  (Fig. 2C).

Last but not least, in addition to controllability in terms of elasticity, the achievable ranges of the charged/uncharged ratios  $\Gamma_X^{\text{st}}$  are constrained by the  $[\text{ATP}]_{\text{tot}} / [\text{GTP}]_{\text{tot}}$  ratio (see Appendix B for details). To

achieve the wide range of charged/uncharged ratios observed *in vivo* [33], cells must regulate not only the driving reactions but also the pool sizes of currency metabolites.

### B. Entropy production rate as a thermodynamic cost

Cellular metabolism requires energy to homeostatically maintain their nonequilibrium states. The coupling of multiple currency metabolites would result in an increase in entropy production rate (EPR) as a thermodynamic cost [34, 35]. The EPR associated with coupling reaction,  $\sigma_{\text{cpl}}$ , is given by [9]

$$\begin{aligned}\sigma_{\text{cpl}} &:= (k_{\text{cpl}}[A][B^*] - k_{\text{cpl}}[A^*][B]) \log \frac{[A][B^*]}{[A^*][B]} \\ &= k_{\text{cpl}}[A]_{\text{tot}}[B]_{\text{tot}} \frac{\Gamma_B - \Gamma_A}{(\Gamma_A + 1)(\Gamma_B + 1)} \log \frac{\Gamma_B}{\Gamma_A}.\end{aligned}$$

It increases with both the difference between  $\Gamma_X$  and the product of currency pool sizes,  $k_{\text{cpl}}[A]_{\text{tot}}[B]_{\text{tot}}$ . Intuitively, the EPR associated with currency coupling can be viewed as the effective “friction” between different currency metabolites (Fig. 1C).

Examining the steady-state (housekeeping) EPR  $\sigma_{\text{cpl}}^{\text{st}}$  in the strong coupling limit ( $k_{\text{cpl}} \gg \kappa_X^{\pm}/[X]_{\text{tot}}$ ) provides further implications into the thermodynamic cost of currency coupling. In this limit, the housekeeping EPR of currency coupling is given by (see Appendix A for derivation):

$$\begin{aligned}\sigma_{\text{cpl}}^{\text{st}} &\simeq \frac{1}{k_{\text{cpl}}} \frac{(\kappa_A^- \kappa_B^+ - \kappa_A^+ \kappa_B^-)^2 [A]_{\text{tot}}[B]_{\text{tot}}}{([A]_{\text{tot}}\kappa_A^+ + [B]_{\text{tot}}\kappa_B^+)([A]_{\text{tot}}\kappa_A^- + [B]_{\text{tot}}\kappa_B^-)} \\ &\propto \frac{1}{k_{\text{cpl}}} \frac{\frac{[A]_{\text{tot}}}{[B]_{\text{tot}}}}{\left(\frac{[A]_{\text{tot}}}{[B]_{\text{tot}}}\kappa_A^+ + \kappa_B^+\right)\left(\frac{[A]_{\text{tot}}}{[B]_{\text{tot}}}\kappa_A^- + \kappa_B^-\right)}, \quad (15)\end{aligned}$$

which depends on the  $[A]_{\text{tot}}/[B]_{\text{tot}}$  ratio, but is independent of the total abundance of currency metabolites,  $[A]_{\text{tot}} + [B]_{\text{tot}}$ . It is maximized at  $[A]_{\text{tot}}/[B]_{\text{tot}} = \sqrt{\kappa_B^+ \kappa_B^-} / \sqrt{\kappa_A^+ \kappa_A^-}$  and decreases as the system deviates from this balanced  $[A]_{\text{tot}}/[B]_{\text{tot}}$  ratio (Fig. 3A).

A similar approximation-based analysis also applies to the weak coupling limit ( $k_{\text{cpl}} \ll \kappa_X^{\pm}/[X]_{\text{tot}}$ ), yielding a qualitatively consistent result: EPR  $\sigma_{\text{cpl}}^{\text{st}}$  increases as the  $[A]_{\text{tot}}/[B]_{\text{tot}}$  ratio approaches 1 (see Appendix A for details).

### C. Tradeoff between elasticity and thermodynamic cost

With strong currency coupling, from Eqs. (11) and (15), the housekeeping EPR  $\sigma_{\text{cpl}}^{\text{st}}$

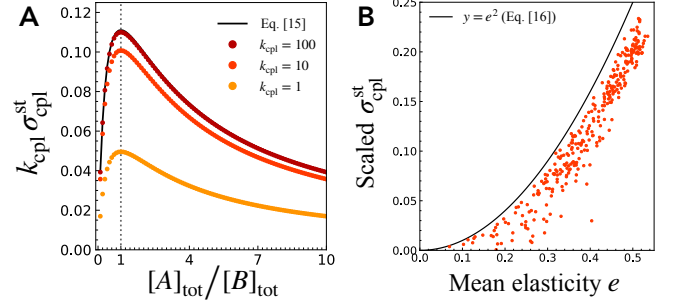


FIG. 3. Thermodynamic cost of currency coupling. (A) Dependence of  $k_{\text{cpl}} \sigma_{\text{cpl}}^{\text{st}}$  on  $[A]_{\text{tot}}/[B]_{\text{tot}}$  with relatively strong currency coupling. The black curve represents the strong coupling limit, Eq. (15). For a consistent comparison, the system size is kept constant by setting  $[A]_{\text{tot}} + [B]_{\text{tot}} = 2$  while  $[A]_{\text{tot}}/[B]_{\text{tot}}$  is varied; parameters are set as  $\kappa_A^+ = 2/3$ ,  $\kappa_A^- = 1/3$ ,  $\kappa_B^+ = 1/3$ ,  $\kappa_B^- = 2/3$ . (B) Relationship between the scaled EPR of the coupling reaction,  $\frac{k_{\text{cpl}} \sqrt{\kappa_A^+ \kappa_A^- \kappa_B^+ \kappa_B^-}}{(\kappa_A^- \kappa_B^+ - \kappa_A^+ \kappa_B^-)^2} \sigma_{\text{cpl}}^{\text{st}}$ , and mean elasticity  $e$ .  $k_{\text{cpl}} = 10$ . The parameters  $\kappa_X^{\pm}$  and  $[X]_{\text{tot}}$  are randomly sampled from a uniform distribution within the range  $[0, 1]$ . The black curve represents the strong coupling limit, Eq. (16).

and elasticity are related as:

$$\sigma_{\text{cpl}}^{\text{st}} \simeq \frac{1}{k_{\text{cpl}}} \frac{(\kappa_A^- \kappa_B^+ - \kappa_A^+ \kappa_B^-)^2}{\sqrt{\kappa_A^+ \kappa_A^- \kappa_B^+ \kappa_B^-}} e^2. \quad (16)$$

It shows a tradeoff such that a higher (lower) mean elasticity is associated with a larger (smaller) EPR. We also numerically confirmed a positive correlation between  $e$  and  $\sigma_{\text{cpl}}^{\text{st}}$  even outside the strong coupling limit (Fig. 3B); thus, this tradeoff could generally appear in systems with a coupling of different currency metabolites. In addition, the following tradeoff inequality holds for arbitrary  $k_{\text{cpl}}$  (see Appendix A for the derivation):

$$\frac{(\kappa_A^- \kappa_B^+ - \kappa_A^+ \kappa_B^-)^2}{k_{\text{cpl}} \sqrt{\kappa_A^+ \kappa_A^- \kappa_B^+ \kappa_B^-}} e^2 \geq \sigma_{\text{cpl}}^{\text{st}}. \quad (17)$$

The tradeoff suggests that greater uniformity in the currency metabolite pools could enhance the controllability of cellular metabolism and thus increase the effective degrees of freedom, at the expense of a higher thermodynamic cost (Fig. 1C). Therefore, organisms inhabiting more complex environments, which require adaptive regulation of metabolic functions in response to higher-dimensional environmental cues, e.g., independent regulation of glycolysis via ATP, citric acid cycle via GTP, and pentose phosphate pathway via NADPH [26], are expected to favor more balanced currency pools during evolution and adaptation (Fig. 1D).

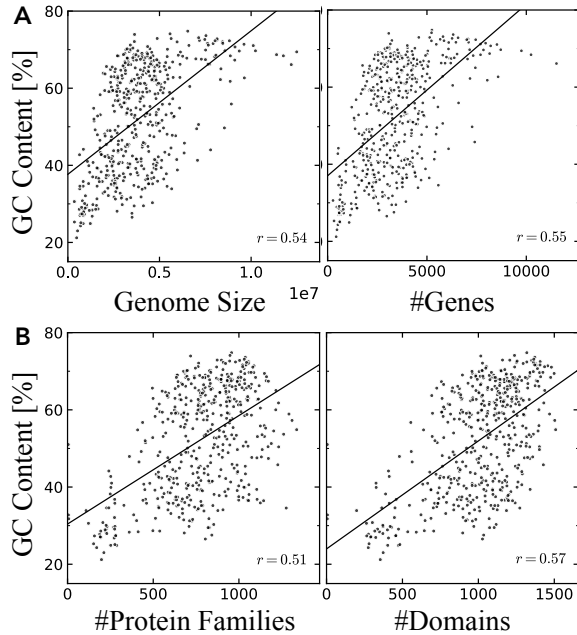


FIG. 4. Statistical relationship between organismal complexity and GC content. (A) Correlation between genomic properties (genome size or the number of coding genes) and GC content. (B) Correlation between proteomic properties (the number of protein families or domains) and GC content. The data are obtained from dataset [36] and Pfam [37] for 496 bacteria and archaea.

#### D. Influence of currency coupling on evolution of GC content

The above tradeoff has various biological implications, including a possible link between ATP–GTP coupling and an evolutionary trend in genomic GC content (see also Fig. 1D).

Genomic GC content refers to the percentage of guanine (G) and cytosine (C) in a genome. Interestingly, the GC content of bacterial genomes is highly diverse, ranging from 15% to 75% across species [36, 38]. Although several factors have been proposed as contributing to this diversity, such as the differential stability due to the number of hydrogen bonds and sugar-acid preference arising from codon usage bias [39, 40], the origin of this diversity remains unknown.

Here, we focus on the statistical relationship between genomic GC content and environmental complexity: GC content generally correlates with various indicators of organismal complexity (Fig. 4). Fig. 4A shows a positive correlation between genomic GC content and the genome size or the number of coding genes—widely-accepted indicators of organismal complexity, or the required complexity of physiological regulation [41, 42]—across diverse microorganisms, as previously reported [43]. GC content also positively correlates with the number of protein families or domains, a recently proposed quantitative indicator of organismal complexity [44] (Fig. 4B).

From an evolutionary perspective, it has been reported that organisms evolve to become GC-poor and AT-rich under simple environmental conditions [43, 45]. Endosymbiotic organisms, which inhabit more stable and simplified environments compared to free-living species, evolve to become GC-poor [38, 46]; similarly, mitochondria and chloroplasts typically have GC-poor genomes [47]. Notably, observations from endosymbiotic evolution [46] suggest the existence of a mechanism that evolutionarily favors low GC content in simple environments, independently of genome size: a sharp reduction in genome size due to gene loss is followed by a progressive decrease in GC content (see Fig. 3 of ref. [46]); in this regime, genome size and GC content are no longer correlated, but GC content continues to decrease as adaptation to “simpler” habitats increases.

Our theory on metabolic currency coupling provides a hypothesis on the evolutionary tendency of GC-poor microbes to inhabit simple environments. NTPs are the building blocks of RNA, which is the second most abundant substance in cells after proteins [48]. Therefore, the intracellular ATP/GTP ratio may be positively correlated with genomic GC content [49] (see also Appendix C). From the perspective of the above controllability–cost tradeoff due to currency coupling, GC-rich microbes should tend to have higher metabolic controllability but higher thermodynamic cost, and *vice versa*. Although GC content may be affected by many other factors, this suggests that microbes in complex habitats should evolve to increase their GC content to enhance metabolic controllability despite the added energetic burden, while microbes in simple habitats should reduce their GC content to lower thermodynamic cost at the expense of controllability (see also Fig. 1D).

## IV. DISCUSSION

This work moves beyond the naïve view that distinct currency metabolites simply regulate distinct functions, instead providing a theoretical basis that quantitatively links the abundances and distributions of multiple currency metabolites to their physiological roles in managing controllability and energetic cost. By developing a minimal model of metabolic currency coupling that does not rely on specific molecules or reactions, we uncover a fundamental tradeoff between the metabolic controllability and the thermodynamic cost: greater controllability of cellular energetic states demands a higher thermodynamic cost, and *vice versa*.

This theory further applies to diverse contexts in both evolution and adaptation. As an evolutionary example, we have argued how metabolic currency coupling could influence the evolutionary trend toward more GC-rich microbes in more complex environments. At the level of non-genetic adaptation, our theoretical results could be experimentally tested by manipulating the pool size of a currency metabolite: e.g., the addition of guano-

sine, which is converted to GTP via the salvage pathway, can increase GTP levels [50]. Note here that, although our minimal model assumes a constant coupling strength  $k_{\text{cpl}}$  for simplicity, parameter values including  $k_{\text{cpl}}$  in reality vary dynamically, depending on enzyme and metabolite abundances or growth conditions. An order-of-magnitude estimation of the parameters in our model suggests that  $k_{\text{cpl}}$  and  $\kappa_{\text{ATP}}^+ / [\text{ATP}]_{\text{tot}}$  are typically of comparable magnitude, both on the order of  $10^3\text{--}10^4$  [M/s] under physiological conditions (see Appendix D for details); this, in turn, implies that both strong and weak currency-coupling regimes can arise in natural cells as well as in experimentally manipulated systems.

Our minimal model simplifies substrates and anabolic products into a single variable  $[F_X^+]$  to capture the essence of metabolic currency coupling. This leads to the unrealistic feature that the total EPR becomes zero in the case without currency coupling ( $k_{\text{cpl}}=0$ ). Such limitations could be resolved by introducing a more detailed and realistic model which incorporates the dynamic change in coupling strength  $k_{\text{cpl}}$  and distinguishes between catabolism and anabolism, without altering our core findings. For example, the present model can be easily extended to systems with the coupling of  $n \geq 3$  currency metabolites, where a similar tradeoff between elasticity and EPR exists (Appendix E).

The present study theoretically examines the monetary economics of energy metabolism, thereby revealing a key tradeoff between metabolic controllability and thermodynamic cost. As viewing biology through the lens of economics has already yielded valuable insight [51–54], we anticipate further intersections between cellular metabolism and monetary economics. For example, the economic theory and observation that a new denomination of currency emerges to reduce temporal and spatial ‘friction’ in the economy [55] seems consistent with the recent theory that the redundancy of currency metabolites (coenzymes) facilitates a parsimonious usage of the proteome [15]. We anticipate that further integrating nonequilibrium chemical thermodynamics, systems biology of metabolism, and mathematical economics will uncover universal constraints and design principles governing the economy of cellular metabolism.

## ACKNOWLEDGMENTS

We would like to thank Ryuna Nagayama for his careful reading of the manuscript. We would also like to acknowledge Kohei Yoshimura, Yuichi Wakamoto, Kenichiro F. Kamei, Naoki Konno, and Takuma Ōnishi for helpful discussions and useful comments. J. F. Y. is supported by the RIKEN Research Fund for Special Postdoctoral Researcher (Project Code: 202501094096), JST ACT-X Grant Number JPMJAX25LG, and the Masason Foundation. T. S. H. is supported by JSPS KAKENHI Grant Number JP21K15048.

## Appendix A: Properties of steady states

The steady state of the present model is calculated as

$$\begin{aligned} [B^*]^{\text{st}} &= \frac{k_{\text{cpl}}[A]_{\text{tot}}\kappa_A^+ + k_{\text{cpl}}[B]_{\text{tot}}\kappa_B^+ + \kappa_A\kappa_B^+}{k_{\text{cpl}}[A]_{\text{tot}}\kappa_A + k_{\text{cpl}}[B]_{\text{tot}}\kappa_B + \kappa_A\kappa_B} [B]_{\text{tot}}, \\ [B]^{\text{st}} &= \frac{k_{\text{cpl}}[A]_{\text{tot}}\kappa_A^- + k_{\text{cpl}}[B]_{\text{tot}}\kappa_B^- + \kappa_A\kappa_B^-}{k_{\text{cpl}}[A]_{\text{tot}}\kappa_A + k_{\text{cpl}}[B]_{\text{tot}}\kappa_B + \kappa_A\kappa_B} [B]_{\text{tot}}, \\ [A^*]^{\text{st}} &= \frac{k_{\text{cpl}}[A]_{\text{tot}}\kappa_A^+ + k_{\text{cpl}}[B]_{\text{tot}}\kappa_B^+ + \kappa_A^+\kappa_B}{k_{\text{cpl}}[A]_{\text{tot}}\kappa_A + k_{\text{cpl}}[B]_{\text{tot}}\kappa_B + \kappa_A\kappa_B} [A]_{\text{tot}}, \\ [A]^{\text{st}} &= \frac{k_{\text{cpl}}[A]_{\text{tot}}\kappa_A^- + k_{\text{cpl}}[B]_{\text{tot}}\kappa_B^- + \kappa_A^-\kappa_B}{k_{\text{cpl}}[A]_{\text{tot}}\kappa_A + k_{\text{cpl}}[B]_{\text{tot}}\kappa_B + \kappa_A\kappa_B} [A]_{\text{tot}}. \end{aligned} \quad (\text{A1})$$

$\Gamma_X^{\text{st}} := [X^*]^{\text{st}} / [X]^{\text{st}}$  ( $1 / \Gamma_X^{\text{st}}$ ) increases linearly with  $\kappa_X^+$  ( $\kappa_X^-$ ), the effective rate constant of the forward (reverse) driving reaction for  $X$  (see Eq. (4)).

The entropy production rate (EPR) of the driving reaction for currency metabolite  $X = A, B$  is given as follows [9]:

$$\begin{aligned} \sigma_X &:= (\kappa_X^-[X^*] - \kappa_X^+[X]) \log \frac{\kappa_X^-[X^*]}{\kappa_X^+[X]} \\ &= \frac{[X]_{\text{tot}}\kappa_X^-}{\Gamma_X + 1} (\Gamma_X - \Gamma_X^\kappa) \log \frac{\Gamma_X}{\Gamma_X^\kappa}, \end{aligned}$$

where  $\Gamma_X^\kappa := \kappa_X^+ / \kappa_X^-$ . That is, the entropy production due to the driving reaction for  $X$  arises from the difference between the charged/uncharged ratio  $\Gamma_X$  of currency metabolite  $X$  and the bias  $\Gamma_X^\kappa = \kappa_X^+ / \kappa_X^-$  in the effective rate constants of forward and reverse driving reactions.

**Weak currency coupling limit.** In the limit of weak currency coupling ( $k_{\text{cpl}} \ll \kappa_X^\pm / [X]_{\text{tot}}$ ), the present model is reduced to a linear dynamical system. The steady state, (A1), is then approximated as:

$$\begin{aligned} [B^*]^{\text{st}} &\simeq [B]_{\text{tot}} \left( \frac{\kappa_B^+}{\kappa_B} + k_{\text{cpl}} \frac{[A]_{\text{tot}}}{\kappa_B} \left( \frac{\kappa_A^+}{\kappa_A} - \frac{\kappa_B^+}{\kappa_B} \right) \right), \\ [B]^{\text{st}} &\simeq [B]_{\text{tot}} \left( \frac{\kappa_B^-}{\kappa_B} + k_{\text{cpl}} \frac{[A]_{\text{tot}}}{\kappa_B} \left( \frac{\kappa_A^-}{\kappa_A} - \frac{\kappa_B^-}{\kappa_B} \right) \right), \\ [A^*]^{\text{st}} &\simeq [A]_{\text{tot}} \left( \frac{\kappa_A^+}{\kappa_A} + k_{\text{cpl}} \frac{[B]_{\text{tot}}}{\kappa_A} \left( \frac{\kappa_B^+}{\kappa_B} - \frac{\kappa_A^+}{\kappa_A} \right) \right), \\ [A]^{\text{st}} &\simeq [A]_{\text{tot}} \left( \frac{\kappa_A^-}{\kappa_A} + k_{\text{cpl}} \frac{[B]_{\text{tot}}}{\kappa_A} \left( \frac{\kappa_B^-}{\kappa_B} - \frac{\kappa_A^-}{\kappa_A} \right) \right). \end{aligned}$$

Notably, the leading-order behavior of  $[X^*]^{\text{st}} / [X]_{\text{tot}}$  and  $[X]^{\text{st}} / [X]_{\text{tot}}$  exhibits no explicit dependence on  $[X]_{\text{tot}}$ . These are primarily governed by the pool size of the other currency metabolite,  $[Y]_{\text{tot}}$  ( $Y \neq X$ ), with the effect of  $[X]_{\text{tot}}$  appearing only at second order.

The same holds for the charged/uncharged ratio and

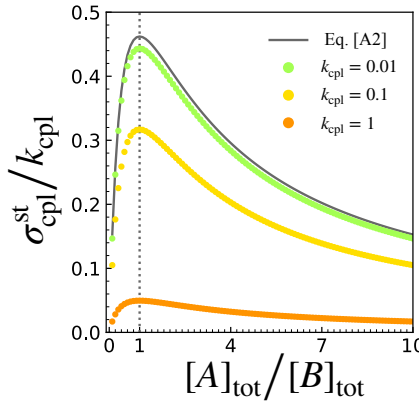


FIG. 5. Dependence of  $\sigma_{\text{cpl}}^{\text{st}}/k_{\text{cpl}}$  on the  $[A]_{\text{tot}}/[B]_{\text{tot}}$  ratio with relatively weak currency coupling (colored points). The gray curve represents (A2). For a consistent comparison, the system size is kept constant by setting  $C_{\text{tot}} = [A]_{\text{tot}} + [B]_{\text{tot}} = 2$  while varying  $[A]_{\text{tot}}/[B]_{\text{tot}}$ ; parameters are set as  $\kappa_A^+ = 2/3$ ,  $\kappa_A^- = 1/3$ ,  $\kappa_B^+ = 1/3$ ,  $\kappa_B^- = 2/3$ .

self-elasticity: e.g., in the case of currency metabolite  $B$ ,

$$\Gamma_B^{\text{st}} \simeq \Gamma_B^{\kappa} + k_{\text{cpl}}[A]_{\text{tot}} \frac{\Gamma_B^{\kappa} + 1}{\Gamma_A^{\kappa} + 1} (\Gamma_A^{\kappa} - \Gamma_B^{\kappa}),$$

$$e_{BB}^{\pm} = 1 - k_{\text{cpl}} \frac{[A]_{\text{tot}} \kappa_A^{\pm}}{\kappa_A \kappa_B^{\pm}} + O(k_{\text{cpl}}^2).$$

This indicates that  $\Gamma_B^{\text{st}}$  is determined by a balance between the effective rate constants,  $\kappa_B^{\pm}$ , of the driving reaction for currency metabolite  $B$  and the driving strength,  $k_{\text{cpl}}[A]_{\text{tot}}$ , of the coupling reaction by the other currency metabolite  $A$ .

As a result,  $\sigma_i^{\text{st}}$  ( $i = A, B, \text{cpl}$ ) are approximated as:

$$\sigma_A^{\text{st}} \simeq k_{\text{cpl}}^2 [A]_{\text{tot}} \frac{\kappa_A^+ \kappa_A^-}{\kappa_A} \left( \frac{[B]_{\text{tot}}}{\kappa_B} \left( \frac{\kappa_B^+}{\kappa_A^+} - \frac{\kappa_B^-}{\kappa_A^-} \right) \right)^2,$$

$$\sigma_B^{\text{st}} \simeq k_{\text{cpl}}^2 [B]_{\text{tot}} \frac{\kappa_B^+ \kappa_B^-}{\kappa_B} \left( \frac{[A]_{\text{tot}}}{\kappa_A} \left( \frac{\kappa_A^+}{\kappa_B^+} - \frac{\kappa_A^-}{\kappa_B^-} \right) \right)^2,$$

$$\sigma_{\text{cpl}}^{\text{st}} \simeq k_{\text{cpl}} [A]_{\text{tot}} [B]_{\text{tot}} \frac{\kappa_A^- \kappa_B^+ - \kappa_A^+ \kappa_B^-}{\kappa_A \kappa_B} \log \frac{\kappa_A^- \kappa_B^+}{\kappa_A^+ \kappa_B^-}. \quad (\text{A2})$$

The non-negative term in (A2),  $\frac{\kappa_A^- \kappa_B^+ - \kappa_A^+ \kappa_B^-}{\kappa_A \kappa_B} \log \frac{\kappa_A^- \kappa_B^+}{\kappa_A^+ \kappa_B^-}$ , quantifies the extent of asymmetry between the effective rate constants of driving reactions,  $\kappa_A^{\pm}$  and  $\kappa_B^{\pm}$ . When normalized by the square of the total currency pool  $C_{\text{tot}} := [A]_{\text{tot}} + [B]_{\text{tot}}$ , the housekeeping EPR of currency coupling,  $\sigma_{\text{cpl}}^{\text{st}}/C_{\text{tot}}^2 \propto k_{\text{cpl}} r/(1 + r)^2$  with  $r := [A]_{\text{tot}}/[B]_{\text{tot}}$ , is maximized at  $r = 1$ . Note here that the total EPR, defined as  $\sigma_{\text{tot}} := \sum_{i=A,B,\text{cpl}} \sigma_i$ , satisfies  $\sigma_{\text{tot}}^{\text{st}} = \sigma_{\text{cpl}}^{\text{st}} + O(k_{\text{cpl}}^2)$  and is primarily governed by the coupling reaction.

Fig. 5 numerically shows that the above approximation (A2) holds well for small  $k_{\text{cpl}}$ . As  $k_{\text{cpl}}$  increases, the (scaled) EPR  $\sigma_{\text{cpl}}^{\text{st}}/k_{\text{cpl}}$  decreases overall and deviates from (A2), but it is still maximized at  $[A]_{\text{tot}}/[B]_{\text{tot}} = 1$ .

**Strong currency coupling limit.** In the limit of strong currency coupling ( $k_{\text{cpl}} \gg \kappa_X^{\pm}/[X]_{\text{tot}}$ ), the charged/uncharged ratios at the steady state are approximated as:

$$\Gamma_A^{\text{st}} = \Gamma_0 + \frac{\kappa_B (\kappa_A^+ - \Gamma_0 \kappa_A^-)}{k_{\text{cpl}} ([A]_{\text{tot}} \kappa_A^- + [B]_{\text{tot}} \kappa_B^-)} + O(k_{\text{cpl}}^{-2}),$$

$$\Gamma_B^{\text{st}} = \Gamma_0 + \frac{\kappa_A (\kappa_B^+ - \Gamma_0 \kappa_B^-)}{k_{\text{cpl}} ([A]_{\text{tot}} \kappa_A^- + [B]_{\text{tot}} \kappa_B^-)} + O(k_{\text{cpl}}^{-2}).$$

Accordingly,

$$\Gamma_B^{\text{st}} - \Gamma_A^{\text{st}} \simeq (\kappa_A^- \kappa_B^+ - \kappa_A^+ \kappa_B^-) \frac{1 + \Gamma_0}{k_{\text{cpl}} ([A]_{\text{tot}} \kappa_A^- + [B]_{\text{tot}} \kappa_B^-)},$$

$$\frac{\Gamma_B^{\text{st}}}{\Gamma_A^{\text{st}}} \simeq 1 + \frac{([A]_{\text{tot}} \kappa_A + [B]_{\text{tot}} \kappa_B) (\kappa_A^- \kappa_B^+ - \kappa_A^+ \kappa_B^-)}{k_{\text{cpl}} ([A]_{\text{tot}} \kappa_A^+ + [B]_{\text{tot}} \kappa_B^+) ([A]_{\text{tot}} \kappa_A^- + [B]_{\text{tot}} \kappa_B^-)}.$$

With the definition of  $\sigma_{\text{cpl}}^{\text{st}}$ , this approximation leads to Eq. (15):

$$\sigma_{\text{cpl}}^{\text{st}} \simeq \frac{1}{k_{\text{cpl}}} \frac{(\kappa_A^- \kappa_B^+ - \kappa_A^+ \kappa_B^-)^2 [A]_{\text{tot}} [B]_{\text{tot}}}{([A]_{\text{tot}} \kappa_A^+ + [B]_{\text{tot}} \kappa_B^+) ([A]_{\text{tot}} \kappa_A^- + [B]_{\text{tot}} \kappa_B^-)}$$

$$\propto \frac{1}{k_{\text{cpl}}} \frac{\frac{[A]_{\text{tot}}}{[B]_{\text{tot}}}}{\left( \frac{[A]_{\text{tot}}}{[B]_{\text{tot}}} \kappa_A^+ + \kappa_B^+ \right) \left( \frac{[A]_{\text{tot}}}{[B]_{\text{tot}}} \kappa_A^- + \kappa_B^- \right)}. \quad (\text{A3})$$

Moreover, from Eq. (A3) and Eq. (12),  $\sigma_{\text{cpl}}^{\text{st}}$  and  $\tilde{e}_X$  are related as

$$\sigma_{\text{cpl}}^{\text{st}} \simeq \frac{(\kappa_A^- \kappa_B^+ - \kappa_A^+ \kappa_B^-)^2}{k_{\text{cpl}} \sqrt{\kappa_A^+ \kappa_A^- \kappa_B^+ \kappa_B^-}} \sqrt{\tilde{e}_A^+ \tilde{e}_A^-} \sqrt{\tilde{e}_B^+ \tilde{e}_B^-} \quad (\text{A4})$$

which leads to Eq. (16). This equation reveals a trade-off: higher (lower) approximate elasticities are associated with larger (smaller) EPR. Given the constraint that the elasticities satisfy  $\tilde{e}_A^+ + \tilde{e}_B^+ = 1$ , the geometric mean  $\tilde{e}_A \tilde{e}_B$  of the elasticities becomes larger when the elasticities  $\tilde{e}_X$  are evenly distributed.

**Tradeoff inequality.** Let us prove the inequality (17).

As  $e = (e_{AA}^+ e_{AA}^- e_{BB}^+ e_{BB}^-)^{1/4} \geq (\tilde{e}_A^+ \tilde{e}_A^- \tilde{e}_B^+ \tilde{e}_B^-)^{1/4}$  holds from Eq. (12), the left-hand side of (17) satisfies

$$\frac{(\kappa_A^- \kappa_B^+ - \kappa_A^+ \kappa_B^-)^2}{k_{\text{cpl}} \sqrt{\kappa_A^+ \kappa_A^- \kappa_B^+ \kappa_B^-}} e^2 \geq \frac{(\kappa_A^- \kappa_B^+ - \kappa_A^+ \kappa_B^-)^2}{k_{\text{cpl}} \sqrt{\kappa_A^+ \kappa_A^- \kappa_B^+ \kappa_B^-}} \sqrt{\tilde{e}_A^+ \tilde{e}_A^-} \sqrt{\tilde{e}_B^+ \tilde{e}_B^-}$$

$$= \frac{[A]_{\text{tot}} [B]_{\text{tot}}}{k_{\text{cpl}}} \frac{(\kappa_A^- \kappa_B^+ - \kappa_A^+ \kappa_B^-)^2}{([A]_{\text{tot}} \kappa_A^+ + [B]_{\text{tot}} \kappa_B^+) ([A]_{\text{tot}} \kappa_A^- + [B]_{\text{tot}} \kappa_B^-)}. \quad (\text{A5})$$

Also, from  $\log x \leq x - 1$ , the right-hand side of (17) satisfies

$$\sigma_{\text{cpl}}^{\text{st}} = k_{\text{cpl}} [A]_{\text{tot}} [B]_{\text{tot}} \frac{\Gamma_B^{\text{st}} - \Gamma_A^{\text{st}}}{(\Gamma_A^{\text{st}} + 1)(\Gamma_B^{\text{st}} + 1)} \log \frac{\Gamma_B^{\text{st}}}{\Gamma_A^{\text{st}}}$$

$$\leq k_{\text{cpl}} [A]_{\text{tot}} [B]_{\text{tot}} \frac{\Gamma_B^{\text{st}} - \Gamma_A^{\text{st}}}{(\Gamma_A^{\text{st}} + 1)(\Gamma_B^{\text{st}} + 1)} \left( \frac{\Gamma_B^{\text{st}}}{\Gamma_A^{\text{st}}} - 1 \right)$$

$$= k_{\text{cpl}} [A]_{\text{tot}} [B]_{\text{tot}} \frac{(\Gamma_B^{\text{st}} - \Gamma_A^{\text{st}})^2}{\Gamma_A^{\text{st}} (\Gamma_A^{\text{st}} + 1)(\Gamma_B^{\text{st}} + 1)}. \quad (\text{A6})$$

Noting that

$$\begin{aligned} \Gamma_B^{\text{st}} - \Gamma_A^{\text{st}} &= \frac{(\kappa_A^- \kappa_B^+ - \kappa_A^+ \kappa_B^-)}{(k_{\text{cpl}}[A]_{\text{tot}} \kappa_A^- + k_{\text{cpl}}[B]_{\text{tot}} \kappa_B^- + \kappa_A^- \kappa_B)} \\ &\quad \times \frac{(k_{\text{cpl}}[A]_{\text{tot}} \kappa_A + k_{\text{cpl}}[B]_{\text{tot}} \kappa_B + \kappa_A \kappa_B)}{(k_{\text{cpl}}[A]_{\text{tot}} \kappa_A^- + k_{\text{cpl}}[B]_{\text{tot}} \kappa_B^- + \kappa_A \kappa_B^-)}, \end{aligned} \quad (\text{A7})$$

it is sufficient to prove

$$\begin{aligned} &\frac{1}{k_{\text{cpl}}^2 ([A]_{\text{tot}} \kappa_A^+ + [B]_{\text{tot}} \kappa_B^+) ([A]_{\text{tot}} \kappa_A^- + [B]_{\text{tot}} \kappa_B^-)} \\ &\geq \frac{1}{(k_{\text{cpl}}[A]_{\text{tot}} \kappa_A^+ + k_{\text{cpl}}[B]_{\text{tot}} \kappa_B^+ + \kappa_A^+ \kappa_B)} \\ &\quad \times \frac{1}{(k_{\text{cpl}}[A]_{\text{tot}} \kappa_A^- + k_{\text{cpl}}[B]_{\text{tot}} \kappa_B^- + \kappa_A \kappa_B^-)}. \end{aligned} \quad (\text{A8})$$

As (A8) is evident, we obtain Eq. (17).

## Appendix B: Bounds on $\Gamma_X$ modulation range

In addition to controllability in terms of elasticity, the achievable ranges of the charged/uncharged ratios  $\Gamma_X^{\text{st}}$  are fundamentally constrained by finite driving strength,  $\kappa_X^\pm$ . If the total driving strength  $\kappa_X = \kappa_X^+ + \kappa_X^-$  has an upper bound  $\kappa_X^{\text{max}}$ ,  $\Gamma_X^{\text{st}}$  is bounded as  $\Gamma_X^{\text{max}} \geq \Gamma_X^{\text{st}} \geq \Gamma_X^{\text{min}}$  with

$$\begin{aligned} \Gamma_X^{\text{max}} &= \frac{\kappa_Y^+}{\kappa_Y^-} + \frac{k_{\text{cpl}}[X]_{\text{tot}} + \kappa_Y}{k_{\text{cpl}}[Y]_{\text{tot}} \kappa_Y^-} \kappa_X^{\text{max}}, \\ \Gamma_X^{\text{min}} &= \left( \frac{\kappa_Y^-}{\kappa_Y^+} + \frac{k_{\text{cpl}}[X]_{\text{tot}} + \kappa_Y}{k_{\text{cpl}}[Y]_{\text{tot}} \kappa_Y^+} \kappa_X^{\text{max}} \right)^{-1}. \quad (Y \neq X) \end{aligned}$$

These upper and lower bounds are governed by the relative magnitudes of  $[X]_{\text{tot}} \kappa_X^\pm$  and  $[Y]_{\text{tot}} \kappa_Y^\pm$ . When the currency metabolite pools are imbalanced ( $[A]_{\text{tot}} \gg [B]_{\text{tot}}$ ), the charged/uncharged ratio  $\Gamma_B^{\text{st}}$  of the less abundant currency metabolite  $B$  is confined to a narrower range  $\Gamma_B^{\text{max}} / \Gamma_B^{\text{min}}$  (Fig. 6), matching the trend observed in the elasticities.

Therefore, to achieve the wide range of charged/uncharged ratios observed *in vivo*, cells must regulate not only the bias  $\kappa_X^+ / \kappa_X^-$  of the driving reactions for currency metabolite  $X$  but also the pool sizes  $[X]_{\text{tot}}$  of currency metabolites.

## Appendix C: On the correlation between the intracellular ATP/GTP ratio and GC content

The intracellular concentration [NTP] of NTPs (i.e., ATP and GTP) is determined by the balance between their production flux  $P_{\text{NTP}}$  and their conversion and dilution:

$$\frac{d}{dt} [\text{NTP}] = P_{\text{NTP}} - k_{\text{NTP}} [\text{NTP}].$$

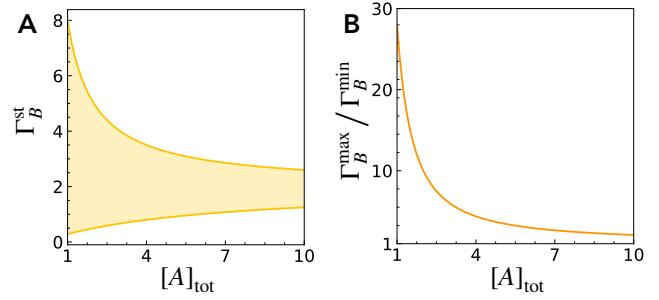


FIG. 6. Dependence of (A)  $\Gamma_B^{\text{st}}$  modulation range,  $[\Gamma_B^{\text{min}}, \Gamma_B^{\text{max}}]$ , and (B) its width,  $\Gamma_B^{\text{max}} / \Gamma_B^{\text{min}}$ , on  $[A]_{\text{tot}}$ .  $\kappa_B = 1$ ,  $k_{\text{cpl}} = 1$ , and  $[B]_{\text{tot}} = 1$  are fixed.

Then, their steady-state concentration is

$$[\text{NTP}]^{\text{st}} = \frac{P_{\text{NTP}}}{k_{\text{NTP}}}.$$

One might reasonably expect the production flux of GTP and guanine to increase with genomic GC content, as supported by experimental evidence [49]. We therefore assume that the production fluxes of ATP and GTP,  $P_{\text{ATP}}$  and  $P_{\text{GTP}}$ , positively correlate with the genomic AT and GC contents, respectively.

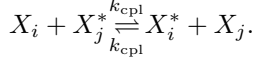
Furthermore, if  $P_{\text{NTP}}$  is decomposed into the flux used for RNA incorporation and that for *de novo* synthesis for currency metabolites, it is natural to assume that only the former is proportional to AT or GC content. Nevertheless, because the pool of free NTPs derived from RNA turnover can greatly exceed that from *de novo* synthesis,  $P_{\text{ATP}}$  and  $P_{\text{GTP}}$  are still expected to correlate positively with AT and GC content, respectively. According to ref. [48], the weight of RNA per cell is about 60 fg, and thus that of ATP or GTP is about 15 fg. In contrast, the intracellular concentrations of ATP and GTP are about 3 mM and 1 mM, respectively [56–58]; because the molecular weights of ATP and GTP are 507 and 523 g/mol and the volume of microbes such as *E. coli* is about  $1 \mu\text{m}^3$ , the weights of (free) ATP and GTP are about 1.5 fg and 0.5 fg, respectively. That is, the intracellular abundance of guanine molecules for RNA is higher by more than an order of magnitude.

## Appendix D: Coupling of $n \geq 3$ Currency Metabolites

As an extension of the minimal model discussed in the main text, we consider a system with  $n \geq 3$  kinds of currency metabolites,  $X_i$  ( $i = 1, 2, \dots, n$ ). Each metabolite  $X_i$  is driven by a reaction with effective rate constants  $\kappa_i^\pm$ :

$$X_i \xrightleftharpoons[\kappa_i^+]{\kappa_i^-} X_i^* \quad (i = 1, 2, \dots, n).$$

These currency metabolites are also assumed to be coupled through exchange reactions of the form[59]:



Assuming mass-action kinetics, the rate equation is given by

$$\begin{aligned} \dot{[X_i^*]} &= \kappa_i^+ [X_i] - \kappa_i^- [X_i^*] + \sum_{i \neq j} k_{\text{cpl}} ([X_i][X_j^*] - [X_i^*][X_j]) \\ &= \kappa_i^+ [X_i]_{\text{tot}} - \kappa_i^- [X_i^*] \\ &\quad + \sum_{j \neq i} k_{\text{cpl}} ([X_i]_{\text{tot}}[X_j^*] - [X_i^*][X_j]_{\text{tot}}), \end{aligned} \quad (\text{D1})$$

where  $\kappa_i := \kappa_i^+ + \kappa_i^-$  ( $i = 1, 2, \dots, n$ ).

**Steady state.** From (D1), the steady state  $[X_i^*]^{\text{st}}$  satisfies

$$(\mathbf{D} + \mathbf{R}) [\mathbf{X}^*]^{\text{st}} = \{\kappa_i^+ [X_i]_{\text{tot}}\}_i,$$

where a diagonal matrix  $\mathbf{D}$  and a rank-one matrix  $\mathbf{R}$  are defined as

$$\mathbf{D} := \text{diag}(\kappa_i + k_{\text{cpl}} C_{\text{tot}})_i, \quad \mathbf{R} := -\{k_{\text{cpl}} [X_i]_{\text{tot}}\}_i \cdot \mathbf{1}^\top,$$

with  $C_{\text{tot}} := \sum_j [X_j]_{\text{tot}}$ .

Therefore, we have:

$$[\mathbf{X}^*]^{\text{st}} = (\mathbf{D} + \mathbf{R})^{-1} \{\kappa_i^+ [X_i]_{\text{tot}}\}_i.$$

Here, the inverse can be evaluated using the matrix inversion lemma (Woodbury matrix identity):

$$\begin{aligned} (\mathbf{D} + \mathbf{R})^{-1} &= \mathbf{D}^{-1} + \\ \mathbf{D}^{-1} \{k_{\text{cpl}} [X_i]_{\text{tot}}\}_i (1 - \mathbf{1}^\top \mathbf{D}^{-1} \{k_{\text{cpl}} [X_i]_{\text{tot}}\}_i)^{-1} \mathbf{1}^\top \mathbf{D}^{-1}. \end{aligned}$$

Accordingly, we obtain:

$$\begin{aligned} [X_i^*]^{\text{st}} &= \frac{[X_i]_{\text{tot}}}{\kappa_i + k_{\text{cpl}} C_{\text{tot}}} \left( \kappa_i^+ + k_{\text{cpl}} \frac{\sum_j \frac{\kappa_j^+ [X_j]_{\text{tot}}}{\kappa_j + k_{\text{cpl}} C_{\text{tot}}}}{1 - \sum_j \frac{k_{\text{cpl}} [X_j]_{\text{tot}}}{\kappa_j + k_{\text{cpl}} C_{\text{tot}}}} \right), \\ [X_i]^{\text{st}} &= \frac{[X_i]_{\text{tot}}}{\kappa_i + k_{\text{cpl}} C_{\text{tot}}} \left( \kappa_i^- + k_{\text{cpl}} \frac{\sum_j \frac{\kappa_j^- [X_j]_{\text{tot}}}{\kappa_j + k_{\text{cpl}} C_{\text{tot}}}}{1 - \sum_j \frac{k_{\text{cpl}} [X_j]_{\text{tot}}}{\kappa_j + k_{\text{cpl}} C_{\text{tot}}}} \right), \\ \Gamma_i^{\text{st}} &:= \frac{[X_i^*]^{\text{st}}}{[X_i]^{\text{st}}} = \frac{\kappa_i^+ + k_{\text{cpl}} \sum_{j \neq i} \frac{(\kappa_i^+ - \kappa_j^+) [X_j]_{\text{tot}}}{\kappa_j + k_{\text{cpl}} C_{\text{tot}}}}{\kappa_i^- + k_{\text{cpl}} \sum_{j \neq i} \frac{(\kappa_j^- - \kappa_i^-) [X_j]_{\text{tot}}}{\kappa_j + k_{\text{cpl}} C_{\text{tot}}}}. \end{aligned} \quad (\text{D2})$$

In the strong coupling limit,

$$\begin{aligned} \Gamma_i^{\text{st}} &= \Gamma_0 + k_{\text{cpl}}^{-1} \frac{\sum_{j \neq i} \kappa_j [X_j]_{\text{tot}} ((\kappa_i^+ - \kappa_j^+) - \Gamma_0 (\kappa_i^- - \kappa_j^-))}{C_{\text{tot}} \sum_j [X_j]_{\text{tot}} \kappa_j^-} \\ &\quad + O(k_{\text{cpl}}^{-2}), \end{aligned} \quad (\text{D3})$$

with

$$\Gamma_0 := \frac{\sum_j [X_j]_{\text{tot}} \kappa_j^+}{\sum_j [X_j]_{\text{tot}} \kappa_j^-}.$$

**Elasticity.** The dimensionless elasticity is defined as

$$e_{ij}^\pm := \pm \frac{\partial \log \Gamma_i^{\text{st}}}{\partial \log \kappa_j^\pm}.$$

Then,

$$\begin{aligned} e_{ii}^\pm &= 1 - \frac{k_{\text{cpl}} \sum_{l \neq i} \frac{\kappa_l^\pm [X_l]_{\text{tot}}}{\kappa_l + k_{\text{cpl}} C_{\text{tot}}}}{\kappa_i^\pm + k_{\text{cpl}} \sum_{l \neq i} \frac{(\kappa_l^\pm - \kappa_i^\pm) [X_l]_{\text{tot}}}{\kappa_l + k_{\text{cpl}} C_{\text{tot}}}}, \\ e_{ij}^\pm &= \frac{k_{\text{cpl}} \frac{\kappa_j^\pm [X_j]_{\text{tot}}}{\kappa_j + k_{\text{cpl}} C_{\text{tot}}}}{\kappa_i^\pm + k_{\text{cpl}} \sum_{l \neq i} \frac{(\kappa_l^\pm - \kappa_i^\pm) [X_l]_{\text{tot}}}{\kappa_l + k_{\text{cpl}} C_{\text{tot}}}} \quad (j \neq i). \end{aligned}$$

Accordingly,  $\sum_j e_{ij}^\pm = 1$ .

In the strong coupling limit,

$$e_{ij}^\pm \rightarrow \tilde{e}_l := \frac{[X_j]_{\text{tot}} \kappa_j^\pm}{\sum_l [X_l]_{\text{tot}} \kappa_l^\pm}.$$

**EPR and tradeoff.** The EPR of all coupling reactions is given by

$$\begin{aligned} \sigma_{\text{cpl}}^{(n)} &:= \sum_{i > j} \sigma_{(i,j)}^{\text{st}} \\ &= \sum_{i > j} k_{\text{cpl}} [X_i]_{\text{tot}} [X_j]_{\text{tot}} \frac{\Gamma_i^{\text{st}} - \Gamma_j^{\text{st}}}{(\Gamma_i^{\text{st}} + 1)(\Gamma_j^{\text{st}} + 1)} \log \frac{\Gamma_i^{\text{st}}}{\Gamma_j^{\text{st}}}. \end{aligned}$$

From (D3), in the strong coupling limit, each  $\sigma_{(i,j)}^{\text{st}}$  can be approximated as:

$$\begin{aligned} \sigma_{(i,j)}^{\text{st}} &\simeq \frac{k_{\text{cpl}}^{-1} [X_i]_{\text{tot}} [X_j]_{\text{tot}}}{(1 + \Gamma_0)^2 \Gamma_0} \left( \frac{d\Gamma_i^{\text{st}}}{dk_{\text{cpl}}^{-1}} \Big|_{k_{\text{cpl}}^{-1} \rightarrow 0} - \frac{d\Gamma_j^{\text{st}}}{dk_{\text{cpl}}^{-1}} \Big|_{k_{\text{cpl}}^{-1} \rightarrow 0} \right)^2 \\ &= \frac{[X_i]_{\text{tot}} [X_j]_{\text{tot}}}{k_{\text{cpl}} (\sum_l [X_l]_{\text{tot}} \kappa_l^+) (\sum_l [X_l]_{\text{tot}} \kappa_l^-)} \times \\ &\quad \left( \frac{\sum_l [X_l]_{\text{tot}} ((\kappa_i^+ - \kappa_j^+) \kappa_l^- - (\kappa_i^- - \kappa_j^-) \kappa_l^+)}{C_{\text{tot}}} \right)^2. \end{aligned}$$

That is,

$$\sigma_{(i,j)}^{\text{st}} \simeq \frac{\left( (\kappa_i^+ - \kappa_j^+) \kappa_l^- - (\kappa_i^- - \kappa_j^-) \kappa_l^+ \right)^2}{k_{\text{cpl}} \sqrt{\kappa_i^+ \kappa_i^-} \sqrt{\kappa_j^+ \kappa_j^-}} \sqrt{\tilde{e}_i^+ \tilde{e}_i^-} \sqrt{\tilde{e}_j^+ \tilde{e}_j^-}, \quad (\text{D4})$$

where  $\bar{\kappa}^\pm := (\sum_l [X_l]_{\text{tot}} \kappa_l^\pm) / (\sum_l [X_l]_{\text{tot}})$  is the averaged effective rate constant of all driving reactions. Therefore, a tradeoff between the EPR  $\sigma_{\text{cpl}}^{(n)}$  and elasticity in the strong coupling limit (analogous to Eq. (16)) still holds, although it is biased by the driving reactions for currency metabolites other than  $X_i$  and  $X_j$ .

Noting the constraint  $\sum_i \tilde{e}_i^\pm = 1$ , (D4) implies that the more uniformly large the values of  $\tilde{e}_i^\pm$  are, the greater the total EPR contributed by all coupling reactions: i.e., an intrinsic tradeoff between global elasticity and thermodynamic cost.

The above results are consistent with the case of  $n = 2$  in the main text.

#### Appendix E: Order estimation of model parameter values

It is thought that cells generally maintain substantial levels of enzymes responsible for metabolic currency coupling. Nucleoside diphosphate kinase (NDPK), for example, is considered a housekeeping enzyme that is constitutively expressed in many types of cells to maintain nucleotide homeostasis [67].

To evaluate the biological relevance of our theory, particularly the controllability–EPR tradeoff relationship, we estimate typical values of relevant parameters and variables, using ATP–GTP coupling as an example (summarized in Table II).

**Effective rate constant of driving reaction.** The total ATP synthesis flux in a microbe is estimated as [58]

$$\kappa_{\text{ATP}}^+[\text{ADP}] \simeq 10^{-2} \text{ [M/s]},$$

and the intracellular ADP concentration in *E. coli* is measured as [60]

$$[\text{ADP}] \simeq 10^{-3} \text{ [M]}.$$

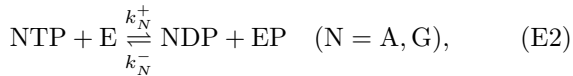
Therefore, the effective rate constant for the driving reaction,  $\text{ADP} \leftrightarrow \text{ATP}$ , should be estimated as

$$\kappa_{\text{ATP}}^+ \simeq 10^1 \text{ [/s].}$$

Given that  $[\text{ATP}]_{\text{tot}} \simeq 3 \times 10^{-3} \text{ [M]}$  [60],

$$\kappa_{\text{ATP}}^+ / [\text{ATP}]_{\text{tot}} \simeq 10^3 \text{--} 10^4 \text{ [/M/s].} \quad (\text{E1})$$

**Coupling constant  $k_{\text{cpl}}$  in ping-pong mechanism.** NDPK catalyzes the following reactions:



in the case of ATP–GTP coupling. Through this ping-pong mechanism, the charged/uncharged ratios,  $\Gamma_{\text{ATP}}$  and  $\Gamma_{\text{GTP}}$ , are driven toward equilibrium, providing an effective coupling between them.

Assuming that reaction (E2) follows mass action kinetics, the steady-state concentrations of E and EP are

calculated as

$$[\text{E}]^{\text{st}} = \frac{k_A[\text{ADP}] + k_G[\text{GDP}]}{k_A[\text{ATP}]_{\text{tot}} + k_G[\text{GTP}]_{\text{tot}}} E_{\text{tot}},$$

$$[\text{EP}]^{\text{st}} = \frac{k_A[\text{ATP}] + k_G[\text{GTP}]}{k_A[\text{ATP}]_{\text{tot}} + k_G[\text{GTP}]_{\text{tot}}} E_{\text{tot}},$$

where  $E_{\text{tot}}$  denotes the total amount of NDPK, and we assume  $k_N := k_N^+ = k_N^-$ .

Accordingly, we obtain the following dynamics of  $[\text{ATP}]$ :

$$\begin{aligned} \frac{d}{dt}[\text{ATP}] &= k_A[\text{ADP}][\text{EP}]^{\text{st}} - k_A[\text{ATP}][\text{E}]^{\text{st}} \\ &\quad + \kappa_A^+[\text{ADP}] - \kappa_A^-[\text{ATP}] \\ &= k_A E_{\text{tot}} \frac{k_G[\text{ADP}][\text{GTP}] - k_G[\text{ATP}][\text{GDP}]}{k_A[\text{ATP}]_{\text{tot}} + k_G[\text{GTP}]_{\text{tot}}} \\ &\quad + \kappa_A^+[\text{ADP}] - \kappa_A^-[\text{ATP}]. \end{aligned}$$

It follows

$$k_{\text{cpl}} = \frac{k_A k_G E_{\text{tot}}}{k_A[\text{ATP}]_{\text{tot}} + k_G[\text{GTP}]_{\text{tot}}}. \quad (\text{E3})$$

From refs. [61–63],

$$\begin{aligned} k_{\text{cat}} &\simeq 10^3 \text{ [/s]}, \\ K_{\text{M,ATP}} &\simeq 10^{-4}\text{--}10^{-3} \text{ [M]}, \\ K_{\text{M,GDP}} &\simeq 10^{-4} \text{ [M]}, \\ E_{\text{tot}} &\simeq 10^{-6} \text{ [M]}, \end{aligned}$$

and thus,

$$k_N \simeq k_{\text{cat}} / K_{\text{M,N}} \simeq 10^6\text{--}10^7 \text{ [/M/s].} \quad (\text{E4})$$

This is consistent with ref. [68], which states that the second order rate constants  $k_N$  for phosphorylation by natural NTPs are between  $0.7\text{--}13 \times 10^6 \text{ [M}^{-1}\text{s}^{-1}]$ .

Finally, from (E3),

$$k_{\text{cpl}} \simeq 10^3\text{--}10^4 \text{ [/M/s].} \quad (\text{E5})$$

From Eqs. (E1) and (E5),  $k_{\text{cpl}}$  and  $\kappa_{\text{ATP}}^+ / [\text{ATP}]_{\text{tot}}$  are typically in the same order of magnitude, while they depend largely on the amount of enzymes and the growth conditions. This order-of-magnitude estimation suggests that  $k_{\text{cpl}}$  and  $\kappa_{\text{ATP}}^+ / [\text{ATP}]_{\text{tot}}$  are of comparable magnitude with typical NDPK concentrations, implying that both strong ( $k_{\text{cpl}} \gg \kappa_{\text{ATP}}^+ / [\text{ATP}]_{\text{tot}}$ ) and weak ( $k_{\text{cpl}} \ll \kappa_{\text{ATP}}^+ / [\text{ATP}]_{\text{tot}}$ ) currency coupling may occur in natural microbial systems. In particular, under nutrient-limited conditions, the strong coupling limit will be more likely.

[1] E. Schrödinger, *What is Life? The Physical Aspect of the Living Cell* (Cambridge Univ Press, 1944).

[2] S. Ornes, How nonequilibrium thermodynamics speaks to

TABLE II. Order estimation in the case of ATP–GTP coupling.

Symbol	Description	Estimated value	Refs.
$[ATP]_{tot}$	Pool size of ATP	1–5 [mM]	[56–58, 60]
$[GTP]_{tot}$	Pool size of GTP	0.1–1 [mM]	[56–58]
$k_{cpl}$	Rate constant for the coupling reaction	$\sim 10^4$ [1/M/s]	[61–63]
$\kappa_{ATP}^\pm$	Effective rate constant for the driving reaction $ADP \rightleftharpoons ATP$	$\sim 10^1$ [1/s]	[58, 60]
$\Gamma_{ATP}$	$[ATP]/[ADP]$ ratio	$1-10^2$	[64, 65]
$\Gamma_{GTP}$	$[GTP]/[GDP]$ ratio	$1-10^2$	[64, 66]
$r$	$[ATP]_{tot}/[GTP]_{tot}$ ratio	$1 - > 10$	[56]

the mystery of life, *Proceedings of the National Academy of Sciences* **114**, 423 (2017).

- [3] L. Von Bertalanffy, The theory of open systems in physics and biology, *Science* **111**, 23 (1950).
- [4] U. von Stockar and L. A. Van der Wielen, *Biothermodynamics: The role of thermodynamics in biochemical engineering* (CRC Press, 2013).
- [5] K. Sekimoto, *Stochastic energetics*, Vol. 799 (Springer, 2010).
- [6] T. Schmiedl and U. Seifert, Stochastic thermodynamics of chemical reaction networks, *The Journal of chemical physics* **126** (2007).
- [7] H. Ge and H. Qian, Mesoscopic kinetic basis of macroscopic chemical thermodynamics: A mathematical theory, *Physical Review E* **94**, 052150 (2016).
- [8] R. Rao and M. Esposito, Nonequilibrium thermodynamics of chemical reaction networks: Wisdom from stochastic thermodynamics, *Physical Review X* **6**, 041064 (2016).
- [9] K. Yoshimura and S. Ito, Information geometric inequalities of chemical thermodynamics, *Physical Review Research* **3**, 013175 (2021).
- [10] Y. Cao and S. Liang, Stochastic thermodynamics for biological functions, *Quantitative Biology* **13**, e75 (2025).
- [11] U. Seifert, Stochastic thermodynamics of single enzymes and molecular motors, *The European Physical Journal E* **34**, 1 (2011).
- [12] R. Rao and L. Peliti, Thermodynamics of accuracy in kinetic proofreading: dissipation and efficiency trade-offs, *Journal of Statistical Mechanics: Theory and Experiment* **2015**, P06001 (2015).
- [13] N. Golubeva and A. Imparato, Efficiency at maximum power of interacting molecular machines, *Physical review letters* **109**, 190602 (2012).
- [14] M. De Bolster, Glossary of terms used in bioinorganic chemistry (iupac recommendations 1997), *Pure and applied chemistry* **69**, 1251 (1997).
- [15] J. E. Goldford, A. B. George, A. I. Flamholz, and D. Segre, Protein cost minimization promotes the emergence of coenzyme redundancy, *Proceedings of the National Academy of Sciences* **119**, e2110787119 (2022).
- [16] J. G. Reich, Energy metabolism of the cell: a theoretical treatise, (No Title) (1981).
- [17] T. S. Hatakeyama and C. Furusawa, Metabolic dynamics restricted by conserved carriers: Jamming and feedback, *PLoS computational biology* **13**, e1005847 (2017).
- [18] R. West, H. Delattre, E. Noor, E. Feliu, and O. S. Soyer, Dynamics of co-substrate pools can constrain and regulate metabolic fluxes, *Elife* **12**, e84379 (2023).
- [19] M. Huss and P. Holme, Currency and commodity metabolites: their identification and relation to the mod-

ularity of metabolic networks, *IET systems biology* **1**, 280 (2007).

- [20] P. Gerlee, L. Lizana, and K. Sneppen, Pathway identification by network pruning in the metabolic network of *escherichia coli*, *Bioinformatics* **25**, 3282 (2009).
- [21] W. S. Jevons, *Money and the Mechanism of Exchange* (D. APPLETON, 1875).
- [22] N. G. Mankiw, *Macroeconomics*, 8th ed. (Worth, 2013).
- [23] C. M. Metallo and M. G. Vander Heiden, Understanding metabolic regulation and its influence on cell physiology, *Molecular cell* **49**, 388 (2013).
- [24] B. J. Koebmann, H. V. Westerhoff, J. L. Snoep, D. Nilsson, and P. R. Jensen, The glycolytic flux in *escherichia coli* is controlled by the demand for atp, *Journal of bacteriology* **184**, 3909 (2002).
- [25] P. S. Bekiaris and S. Klamt, Network-wide thermodynamic constraints shape nad (p) h cofactor specificity of biochemical reactions, *Nature Communications* **14**, 4660 (2023).
- [26] R. West, Sonal, T. D. Rodrigues, W. Shou, and O. S. Soyer, Asymmetric co-substrate usage at a metabolic branch point can drive overflow metabolism, *bioRxiv* , 2025 (2025).
- [27] A. Wittinghofer and I. R. Vetter, Structure-function relationships of the g domain, a canonical switch motif, *Annual review of biochemistry* **80**, 943 (2011).
- [28] N. Mrnjavac and W. F. Martin, Gtp before atp: The energy currency at the origin of genes, *Biochimica et Biophysica Acta (BBA)-Bioenergetics* **1866**, 149514 (2025).
- [29] W. Ying, Nad+/nadh and nadp+/nadph in cellular functions and cell death: regulation and biological consequences, *Antioxidants & redox signaling* **10**, 179 (2008).
- [30] C. Cantó, K. J. Menzies, and J. Auwerx, Nad+ metabolism and the control of energy homeostasis: a balancing act between mitochondria and the nucleus, *Cell metabolism* **22**, 31 (2015).
- [31] I. Lascu and P. Gonin, The catalytic mechanism of nucleoside diphosphate kinases, *Journal of bioenergetics and biomembranes* **32**, 237 (2000).
- [32] P. Samuelson, *Foundations of economic analysis*, Harvard Economic Studies (Oxford University Press, 1947).
- [33] M. Liesa and O. S. Shirihi, Mitochondrial dynamics in the regulation of nutrient utilization and energy expenditure, *Cell metabolism* **17**, 491 (2013).
- [34] Y. Himeoka and K. Kaneko, Entropy production of a steady-growth cell with catalytic reactions, *Physical Review E* **90**, 042714 (2014).
- [35] M. J. Droste, M. Remeijer, R. Planqué, and F. J. Bruggeman, Thermodynamics of unicellular life: Entropy production rate as function of the balanced growth rate, *bioRxiv* , 2024 (2024).

[36] J. S. Madin, D. A. Nielsen, M. Brbic, R. Corkrey, D. Danko, K. Edwards, M. K. Engqvist, N. Fierer, J. L. Geoghegan, M. Gillings, *et al.*, A synthesis of bacterial and archaeal phenotypic trait data, *Scientific data* **7**, 170 (2020).

[37] J. Mistry, S. Chuguransky, L. Williams, M. Qureshi, G. A. Salazar, E. L. Sonnhammer, S. C. Tosatto, L. Paladin, S. Raj, L. J. Richardson, *et al.*, Pfam: The protein families database in 2021, *Nucleic acids research* **49**, D412 (2021).

[38] E. P. Rocha and A. Danchin, Base composition bias might result from competition for metabolic resources, *TRENDS in Genetics* **18**, 291 (2002).

[39] N. Sueoka, Correlation between base composition of deoxyribonucleic acid and amino acid composition of protein, *Proceedings of the National Academy of Sciences* **47**, 1141 (1961).

[40] M. Gralka, S. Pollak, and O. X. Cordero, Genome content predicts the carbon catabolic preferences of heterotrophic bacteria, *Nature Microbiology* **8**, 1799 (2023).

[41] C. E. Nelson, B. M. Hersh, and S. B. Carroll, The regulatory content of intergenic dna shapes genome architecture, *Genome biology* **5**, 1 (2004).

[42] A. A. Sharov, Genome increase as a clock for the origin and evolution of life, *Biology Direct* **1**, 1 (2006).

[43] A. Almanpis, M. Swain, D. Gatherer, and N. McEwan, Correlation between bacterial g+ c content, genome size and the g+ c content of associated plasmids and bacteriophages, *Microbial genomics* **4** (2018).

[44] D. Alvarez-Ponce and S. Krishnamurthy, Organismal complexity strongly correlates with the number of protein families and domains, *Proceedings of the National Academy of Sciences* **122**, e2404332122 (2025).

[45] K. U. Foerstner, C. Von Mering, S. D. Hooper, and P. Bork, Environments shape the nucleotide composition of genomes, *EMBO reports* **6**, 1208 (2005).

[46] J. P. McCutcheon, B. M. Boyd, and C. Dale, The life of an insect endosymbiont from the cradle to the grave, *Current Biology* **29**, R485 (2019).

[47] T. Zhang, Y. Fang, X. Wang, X. Deng, X. Zhang, S. Hu, and J. Yu, The complete chloroplast and mitochondrial genome sequences of boea hygrometrica: insights into the evolution of plant organellar genomes, *PLoS One* **7**, e30531 (2012).

[48] R. Milo and R. Phillips, *Cell biology by the numbers* (Garland Science, 2015).

[49] A.-K. Dietel, H. Merker, M. Kaltenpoth, and C. Kost, Selective advantages favour high genomic at-contents in intracellular elements, *PLoS genetics* **15**, e1007778 (2019).

[50] A. Kriel, A. N. Bittner, S. H. Kim, K. Liu, A. K. Tehranchi, W. Y. Zou, S. Rendon, R. Chen, B. P. Tu, and J. D. Wang, Direct regulation of gtp homeostasis by (p) ppGPP: a critical component of viability and stress resistance, *Molecular cell* **48**, 231 (2012).

[51] The Economic Cell Collective, *Economic Principles in Cell Biology* (No commercial publisher, Online open access book, 2026).

[52] J. F. Yamagishi and T. S. Hatakeyama, Microeconomics of metabolism: The warburg effect as giffen behaviour, *Bulletin of Mathematical Biology* **83**, 1 (2021).

[53] J. F. Yamagishi and T. S. Hatakeyama, Linear response theory of evolved metabolic systems, *Physical Review Letters* **131**, 028401 (2023).

[54] J. F. Yamagishi and T. S. Hatakeyama, Global constraint principle for microbial growth laws, *Proceedings of the National Academy of Sciences* **122**, e2515031122 (2025).

[55] A. Kuroda, *A global history of money* (Routledge, 2020).

[56] A. Danchin, L. Dondon, and J. Daniel, Metabolic alterations mediated by 2-ketobutyrate in escherichia coli k12, *Molecular and General Genetics MGG* **193**, 473 (1984).

[57] M. C. Jewett, M. L. Miller, Y. Chen, and J. R. Swartz, Continued protein synthesis at low [atp] and [gtp] enables cell adaptation during energy limitation, *Journal of bacteriology* **191**, 1083 (2009).

[58] Y. Deng, D. R. Beahm, S. Ionov, and R. Sarpeshkar, Measuring and modeling energy and power consumption in living microbial cells with a synthetic atp reporter, *BMC biology* **19**, 101 (2021).

[59] The following analysis can be applied to systems in which the coupling constant varies among currency metabolite pairs.

[60] K. R. Albe, M. H. Butler, and B. E. Wright, Cellular concentrations of enzymes and their substrates, *Journal of theoretical biology* **143**, 163 (1990).

[61] D. Zala, U. Schlattner, T. Desvignes, J. Bobe, A. Roux, P. Chavrier, and M. Boissan, The advantage of channeling nucleotides for very processive functions, *F1000Research* **6**, 724 (2017).

[62] M. Tokarska-Schlattner, M. Boissan, A. Munier, C. Borot, C. Mailleau, O. Speer, U. Schlattner, and M.-L. Lacombe, The nucleoside diphosphate kinase d (nm23-h4) binds the inner mitochondrial membrane with high affinity to cardiolipin and couples nucleotide transfer with respiration, *Journal of Biological Chemistry* **283**, 26198 (2008).

[63] J. D. Pollack, M. A. Myers, T. Dandekar, and R. Herrmann, Suspected utility of enzymes with multiple activities in the small genome mycoplasma species: the replacement of the missing “household” nucleoside diphosphate kinase gene and activity by glycolytic kinases, *Omics: a journal of integrative biology* **6**, 247 (2002).

[64] T. W. Traut, Physiological concentrations of purines and pyrimidines, *Molecular and cellular biochemistry* **140**, 1 (1994).

[65] M. Tantama, J. R. Martínez-François, R. Mongeon, and G. Yellen, Imaging energy status in live cells with a fluorescent biosensor of the intracellular atp-to-adp ratio, *Nature communications* **4**, 2550 (2013).

[66] S. Colombo, P. Ma, L. Cauwenberg, J. Winderickx, M. Crauwels, A. Teunissen, D. Nauwelaers, J. H. de Winde, M.-F. Gorwa, D. Colavizza, *et al.*, Involvement of distinct g-proteins, gpa2 and ras, in glucose-and intracellular acidification-induced camp signalling in the yeast saccharomyces cerevisiae, *The EMBO journal* (1998).

[67] H. Yu, X. Rao, and K. Zhang, Nucleoside diphosphate kinase (ndk): a pleiotropic effector manipulating bacterial virulence and adaptive responses, *Microbiological Research* **205**, 125 (2017).

[68] S. Schaerli, M. Konrad, and M. A. Geeves, Substrate specificity of human nucleoside-diphosphate kinase revealed by transient kinetic analysis, *Journal of Biological Chemistry* **273**, 5662 (1998).